



Flow Characterization and Modeling of Strong Round Synthetic Jets in Crossflow

Xi Xia* and Kamran Mohseni†
University of Florida, Gainesville, Florida 32611-6250

DOI: 10.2514/1.J054880

This study focuses on the flow field of a round synthetic jet issuing into a crossflow. Six cases are investigated in which the jet-to-freestream velocity ratios range between 2.8 and 8.3. This corresponds to a medium-to-strong transverse jet, which is characterized using both two-dimensional hot-wire anemometry and particle image velocimetry techniques. A self-similar model is developed for the centerline trajectory and velocity of a transverse synthetic jet. The resulting scaling laws are validated with experimental data. The scaling coefficients are found to be independent of the synthetic jet strength (characterized by the stroke ratio) for large-velocity-ratio cases, provided that the jet velocity is calculated based on the momentum flux of the leading vortex ring of the synthetic jet. Furthermore, the velocity component parallel to the crossflow is enhanced over the crossflow velocity in the near field and fundamentally different from continuous jets. This can be explained by the induced effect of the asymmetric vortex rings in the near field, which are a result of the interaction between the crossflow and the synthetic jet.

Nomenclature

A_f	=	far-field trajectory coefficient
A_n	=	near-field trajectory coefficient
A_s	=	characteristic area of jet cross section, m ²
B	=	cavity depth of the synthetic jet actuator, mm
B_f	=	far-field w -velocity coefficient
B_n	=	near-field w -velocity coefficient
D	=	cavity diameter of the synthetic jet actuator, mm
d	=	orifice diameter of the synthetic jet actuator, mm
f	=	jet driving frequency, Hz
L	=	stroke length, mm
$\Delta \dot{M}_x$	=	x -component momentum deficit, N
\dot{M}_z	=	z -component momentum flux, N
\dot{m}	=	mass flux, kg/s
n	=	unit vector normal to the jet centerline
Re_s	=	Reynolds number at the synthetic jet exit
r	=	jet-to-freestream velocity ratio
s	=	unit vector tangential to the jet centerline
U	=	mean flow velocity, m/s
u	=	x -component velocity, m/s
u_∞	=	crossflow velocity, m/s
w	=	z -component velocity, m/s
w_j	=	effective jet velocity, m/s
x	=	direction parallel to the crossflow
x_c	=	x coordinate of the jet centerline, mm
z	=	direction perpendicular to the crossflow
z_c	=	z coordinate of the jet centerline, mm
α	=	angle between the measured flow and the hot-wire probe axis, deg
Δ	=	peak-to-peak deflection of the piezoelectric membrane, μm
Γ	=	circulation of a vortex, m ² /s
ν	=	dynamic viscosity, (N · s)/m ²

I. Introduction

THE synthetic jet [1–4] is a unique type of jet as its formation does not require an internal flow source. For this reason, it is also called a zero-net-mass-flux (ZNMF) jet. The mechanism of a synthetic jet resembles the propulsive technique of squids or cephalopods [5,6], which create a net-momentum-flux flow by periodically taking in fluid from the surroundings and then ejecting high-momentum shear layers that roll into vortex rings. It is the vortex-ring formation that fundamentally distinguishes synthetic jets from continuous jets. The formation process for a starting vortex ring has been studied by Maxworthy [7], Saffman [8], Didden [9], Glezer [10], and Gharib and his colleagues [11–13] among others. Later, research interests have been focused on the basic flow of synthetic jets issued into a quiescent environment. In the near field of a synthetic jet, Smith and Glezer [1] and Smith and Swift [14] have found that the jet formation and evolution is dictated by a nondimensional stroke ratio, which is the reciprocal of the Strouhal number. Holman et al. [15] found that the stroke ratio dictates the jet formation criterion. However, the far-field flow seems to depend on both the stroke ratio and the Reynolds number [14,16,17]. In the far field, the scaled-mean-velocity and turbulent-intensity profiles of all synthetic jets can be collapsed onto a single self-similar profile [1,18–20]. Because self-similarity is also an intrinsic feature for the far field of continuous jets, we recently proposed a unified approach [17] to model the far field of both continuous and synthetic jets. Another striking feature of synthetic jets lies in their enhanced entrainment and mixing compared with continuous jets [14,21,22], which can be modeled by an enhanced effective eddy viscosity associated with the synthetic jet [19].

Because of the absence of any flow sources as well as enhanced entrainment and mixing, synthetic jets have been widely used in a variety of applications [3,4] such as propulsion and maneuvering [6,23], separation control of boundary layers [24–28], as well as flow control over airfoils [29–34]. Recently, synthetic jets have also been used as acoustic liners that are activated in the resonant mode to dissipate acoustic energy in engine ducts [35]. In many synthetic-jet flow control applications, the actuator operates by issuing a synthetic jet into a background crossflow. This operational principle is supported by the finding that the interaction between a synthetic jet and crossflow could facilitate momentum transfer between inside and outside of the boundary layer [36–39], and further change the pressure distribution of external flow [25,30,40,41] or modify the vorticity distribution of the flow field [27,31,42,43]. Therefore, studying the flow field of a synthetic jet in crossflow is necessary in understanding the control effect of synthetic jet actuators.

Previous experimental [36,43–49] and numerical [42,48,50–54] investigations of a transverse synthetic jet have focused on the

Received 11 November 2015; revision received 27 June 2016; accepted for publication 28 June 2016; published online 31 October 2016. Copyright © 2016 by the American Institute of Aeronautics and Astronautics, Inc. All rights reserved. All requests for copying and permission to reprint should be submitted to CCC at www.copyright.com; employ the ISSN 0001-1452 (print) or 1533-385X (online) to initiate your request. See also AIAA Rights and Permissions www.aiaa.org/randp.

*Graduate Research Assistant, Department of Mechanical and Aerospace Engineering. Student Member AIAA.

†William P. Bushnell Endowed Chair in Mechanical and Aerospace Engineering Department and Electrical and Computer Engineering Department; mohseni@ufl.edu. Associate Fellow AIAA.

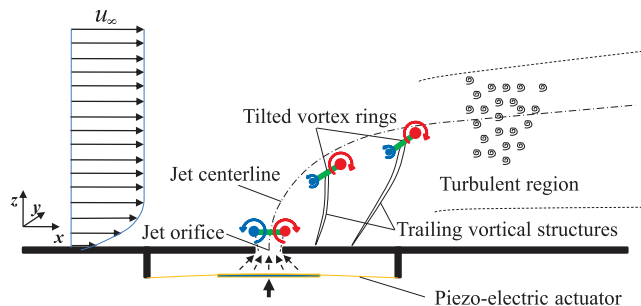


Fig. 1 Schematic showing the 2D flow field of the center plane of a round synthetic jet in a crossflow.

interaction of the jet with the crossflow boundary layer. These publications provide an understanding about the vortex generation and evolution as well as the mean flow features in the near-wall region. Specifically, as shown in Fig. 1, Yehoshua and Seifert [44] and Jabbar and Zhong [43] have found that the interaction between the crossflow and a vortex ring would modify the vorticity distribution of the vortex in an asymmetric manner and rotate the vortex ring axis toward the upstream of the crossflow. The majority of these studies generally share two common features: a relatively weak jet strength compared with the crossflow (a jet-to-crossflow velocity ratio of approximately 1 or less) and a jet penetration depth that is comparable to boundary-layer thickness. To this end, the studies of weak jets are primarily related to the applications of boundary-layer control. However, for vehicle propulsion or maneuvering, vortex thrusters could operate in the regime of transverse synthetic jets with medium-to-large velocity ratios. Among the limited literature on this subject, previous studies [55–57] have mainly investigated the mean flow field to obtain the penetration and centerline trajectory of strong synthetic jets (velocity ratio much larger than 1). In an attempt to promote the study of strong synthetic jets in crossflow, this study will develop a similarity model for the centerline trajectory and velocity of a strong synthetic jet in a near-uniform crossflow, which has a thin laminar boundary layer. The motivation for this model is twofold. One comes from the proven models of a transverse continuous jet, for which similarity analysis [58,59] has been applied to derive scaling laws for velocity, scalar concentration, and jet trajectory. The second originates from a series of synthetic-jet studies [19,20,57,60] that seek self-similarity solutions of synthetic jets based on relevant models of continuous jets. Because the far fields of continuous jets and synthetic jets resemble each other if scaled properly [17], it is possible to extend the solution for a transverse continuous jet to the case of a synthetic jet in the current study.

Previous experimental studies have applied particle image velocimetry (PIV) [43,44,46–48,61] and hot-wire anemometry (HWA) [36,44,45,56] for flow-field characterization. The HWA is primarily used for sampling the mean flow, whereas the PIV enables instantaneous velocity measurement to help understand the formation and evolution of the vortical structures. In this study, both two-dimensional (2D) HWA and phase-locked PIV will be applied for flow-field measurement. However, as discussed here, the accuracy of the HWA would decrease as the angle between the probe axis and the mean velocity of the measured flow increases. To overcome this difficulty in measuring the 2D flow in the center plane of a transverse synthetic jet, a rotary stage together with an iterative angle-detection scheme was applied to automatically align the probe axis with the flow direction for each sampling location.

This paper is organized as follows. Section II introduces the experimental approaches for measuring the 2D jet flow using HWA and PIV. Section III presents the preliminary results of the flow field for different cases of transverse synthetic jets. Section IV provides the self-similar models for the centerline trajectory and velocity of a transverse synthetic jet, and the model for estimating the effective synthetic jet velocity. Section V presents the model validation for the proposed centerline trajectory and velocity relations, as well as physical analysis and discussions. Our final conclusions are given in Sec. VI.

II. Experimental Approaches

A. Experimental Setup

To experimentally characterize the flow field of transverse synthetic jets, the background crossflow is created by an engineering laboratory design (ELD) wind tunnel at the University of Florida. This is a closed-circuit, low-Reynolds-number wind tunnel, the velocity of which can be maintained between 1 and 90 m/s using a PID controller, with an uncertainty within 0.05 m/s. For present study, the flow temperature is maintained at 20°C. The tunnel houses a 0.61 m × 0.61 m × 2.44 m test section, inside which the necessary apparatus for generating the synthetic jet and acquiring the flow-field data are mounted.

The synthetic jet is created from a circular cavity sealed by a piezoelectric disk on one end, and is connected to the surrounding fluid through a round jet orifice on the other. The diameter (D) and depth (B) of the cavity are 33.5 and 2 mm, respectively, whereas the orifice has a diameter (d) of 2 mm and a thickness of 1 mm. A sinusoidal voltage is applied on the piezoelectric material to drive the oscillatory motion of the disk and causes the periodic suction and ejection behaviors of the actuator. The jet strength can be controlled by adjusting the amplitude and frequency of the driving voltage, and quantified by the nondimensional stroke ratio, L/d , where the stroke length L is the equivalent length of a hypothetical cylindrical fluid slug coming out of the actuator orifice in each stroke. According to Krishnan and Mohseni [19], $L = \alpha_p \Delta D^2 / d^2$, where α_p is a constant and Δ is the peak-to-peak deflection of the piezoelectric membrane. Here, Δ is measured with a laser nano-sensor (LMI LNS type 4), similar to that used in previous studies [16,19]. The total uncertainty associated with the calculation of L/d is around 10%.

As shown in Fig. 2, the synthetic jet actuator is mounted flush to one side of a 30 cm × 20 cm × 0.5 cm acrylic flat plate, which is placed vertically inside the wind tunnel and parallel to the background flow. In this way, the synthetic jet is issued perpendicular to the flow of the wind-tunnel test section, and forms a transverse synthetic jet. The traverse system is mounted on the floor of the wind tunnel and the blockage is about 2% of the tunnel cross section. For clarity, the stage dimensions are exaggerated in Fig. 2. The probe support creates a vertical distance of 0.3 m between the traverse system and the flow measurement plane, and so the blockage effect is negligible. As will be discussed in Sec. IV, the transverse jet model in the current study requires the background flow to be uniform, at least in the self-similar region of a synthetic jet (starting $10d \sim 15d$ away from the jet exit). Therefore, it is desirable to have a crossflow with a thin laminar boundary layer. For this purpose, the flat plate has been designed to have a smooth leading edge (elliptical shape with an aspect ratio of 10) to avoid any disturbances or flow separation. This gives a boundary-layer thickness (δ) of less than $3d$ near the jet exit according to the Blasius boundary-layer estimation, which matches well with the experimental data as shown in Fig. 3. Based on the Blasius boundary layer, we estimate the momentum thickness (θ) to be $0.32d$, $0.22d$, and $0.18d$ for crossflow speeds of 2, 4, and 6 m/s, respectively.

Experiments were conducted with different combinations of crossflow velocities and synthetic jet strengths. While the strength of

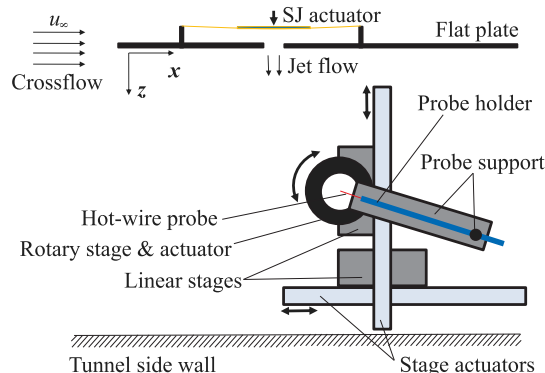


Fig. 2 Schematic showing the top view of the HWA system (out of scale).

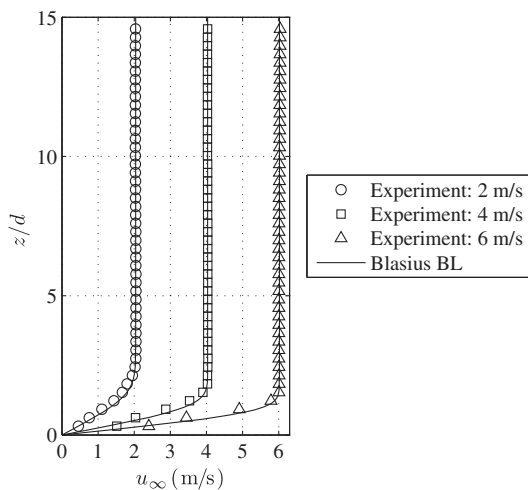


Fig. 3 The crossflow velocity profiles at the streamwise location of the jet exit, for different wind tunnel speeds of 2, 4, and 6 m/s. This velocity data were obtained through PIV measurement.

the synthetic jet was adjusted through L/d , the velocity of the crossflow was controlled by setting the speed of the wind tunnel, which has an average turbulence intensity of less than 0.5% for this experiment. Table 1 summarizes different test cases and their controlling parameters.

B. Velocity Measurement

Although the velocity field of a transverse synthetic jet is generally three-dimensional (3D), here we focus on the flow field of the center plane (x - z plane), which is a 2D flow and can be measured using an x -shaped hot-wire probe (Dantec 55P51). Both wires are calibrated with fourth-order polynomial curves following an iterative procedure [62]. This calibration method is based on regulating a tube flow at constant flow rates, and then iteratively matching the regulated flow rates with the velocity profiles measured with HWA. This method allows accurate calibration at velocities much lower than normal pressure transducers. The result is an uncertainty of 2% for measured velocity $U > 1$ m/s and 20% for $U < 0.2$ m/s. The x -shaped hot-wire probe, as illustrated in Fig. 4a, is designed to measure 2D flows, where the angle between the mean flow and the probe axis is less than 45 deg. However, the accuracy of this measurement drops as the flow angle α increases. This is demonstrated in Fig. 4b, which plots the variations of the velocity-magnitude error (δ_U) and the flow-angle error (δ_α) with α . This inaccuracy caused by a nonzero α has two primary sources, one of which is related to the error in measuring the yaw coefficient [63] for both hot wires, and the other is attributable to the error in aligning the probe axis with the incoming flow during calibration. However, these errors can be eliminated if $\alpha \rightarrow 0$ deg. In this experiment, $\alpha \rightarrow 0$ deg is achieved by affixing the hot-wire probe to a holder positioned on a motorized rotary stage. We then apply an iterative stage-control algorithm to automatically rotate the hot-wire probe to reduce α , so that the probe axis becomes aligned with the local mean velocity vector. The setup for obtaining the flow field of a transverse synthetic jet is also shown in Fig. 2, in which the rotary stage is mounted on top of a linear traverse system. This traverse system is composed of two motorized linear stages that are

perpendicular to each other and traverse in the x - z plane. To acquire the flow field, the stages are programmed and moved in discrete intervals in the x and z directions. At each location the iterative stage-control scheme is first performed to align the probe axis with the local mean flow and then the flow is sampled for 10 s at a rate of 50 kHz.

For comparison and resolving the time-dependent vortical structures, a PIV system is also employed to measure the same 2D flow at the center plane of the transverse synthetic jets. This system uses a high-speed CMOS camera (Phantom v210; 1280×800 px², over 2000 fps) and a 20 mJ Nd:YLF laser (Quantronix Darwin Duo; $\gamma = 527$ nm, repetitions up to 10 kHz). Olive oil particles (~ 1 μ m) are generated by an atomizer to seed the flow field. For each test, the camera and the laser are synchronized through the Insight 4G software by TSI Inc. to acquire the image pairs at a rate of $f/10$ for 2 s (a total of 360–380 images depending on the jet actuation frequency f). The trigger for the synthetic jet is synchronized with the PIV system and the trigger delay is adjusted to obtain the instantaneous flow field of the jet locked at a desired phase (10 per cycle), similar to what was demonstrated by Yehoshua and Seifert [44]. Therefore, a time-averaged flow field can be obtained by averaging the phase-locked data of each cycle.

III. Preliminary Results

The modeling approach in this study, as will be introduced in Sec. IV, is built on the mean velocity field of the center plane of a transverse synthetic jet. In this section, we first present the flow field obtained through HWA and PIV measurements to validate our experimental approach and provide a basic understanding of the mean flow features. Then, the flow field data are analyzed to give the centerline trajectory, which is compared among different cases to imply the bending characteristics.

A. Mean Flow Field

We start by showing streamlines of the mean flow field obtained from PIV for two sample cases (cases 3 and 5) in Fig. 5. We then compare HWA and PIV measurements by plotting the velocity magnitude contours and vectors in Figs. 6 and 7. To optimize the sampling efficiency of the HWA measurement, the sampling region is pre-estimated to include only the mainstream of the jet flow so that the sampling grid becomes nonuniform. For comparison purposes, the PIV data in Figs. 6 and 7 are obtained by interpolating the original higher resolution data to the sampling locations of the corresponding HWA tests. Qualitatively agreement between HWA and PIV measurements can be observed from the streamline and the velocity vector plots. However, the PIV data seem to display a thinner jet region compared with the HWA data in the velocity magnitude contours. This reflects the size effect of the x -shaped hot-wire sensor, which may overestimate the velocities near but outside the core region of a jet, consequently expanding the core region. Further comparison of the performance between HWA and PIV measurements will be provided in the following sections.

As observed from the contour plots in Figs. 6 and 7, the flow field of a transverse synthetic jet resembles a typical jet in that it has a core region near the jet exit; however, it is asymmetric and deflected to some extent. This apparent jet region extends only up to $z = 15d$ or so, where the mainstream of the jet flow starts to bend significantly and turn into the crossflow. This differentiation is used to identify two dynamically different regions for the case of a continuous jet, namely, the jet-dominated domain and the crossflow-dominated domain. To account for the unique vortex formation effect in the jet-dominated region, the flow field of a transverse synthetic jet can be divided into three regions: I) the synthetic jet region, II) the near field, and III) the far field. In the synthetic jet region (I), which is the region immediately outside the jet orifice with $z < 5d$, the flow is dominated by the periodic process of suction and vortex formation. This region generally corresponds to the near field of a synthetic jet in static flow. However, as reported by Yehoshua and Seifert [44] and Jabbar and Zhong [43], the formed vortex ring is asymmetric under the influence of the crossflow as opposed to a free synthetic jet. In the near field (II), the region ($5d \leq z \leq 15d$) where an equivalent free synthetic jet

Table 1 Test matrix displaying the jet driving frequency (f), jet stroke ratio (L/d), jet Reynolds number ($Re_s = \sqrt{2}fLd/\nu$ [19]), and crossflow velocity (u_∞)

Case	f , Hz	L/d	Re_s	u_∞ , m/s
1	1800	2.8	1869	2.0
2	1800	3.7	2481	2.0
3	1900	4.6	3289	2.0
4	1850	5.7	3981	2.0
5	1850	5.7	3981	4.0
6	1850	5.7	3981	6.0

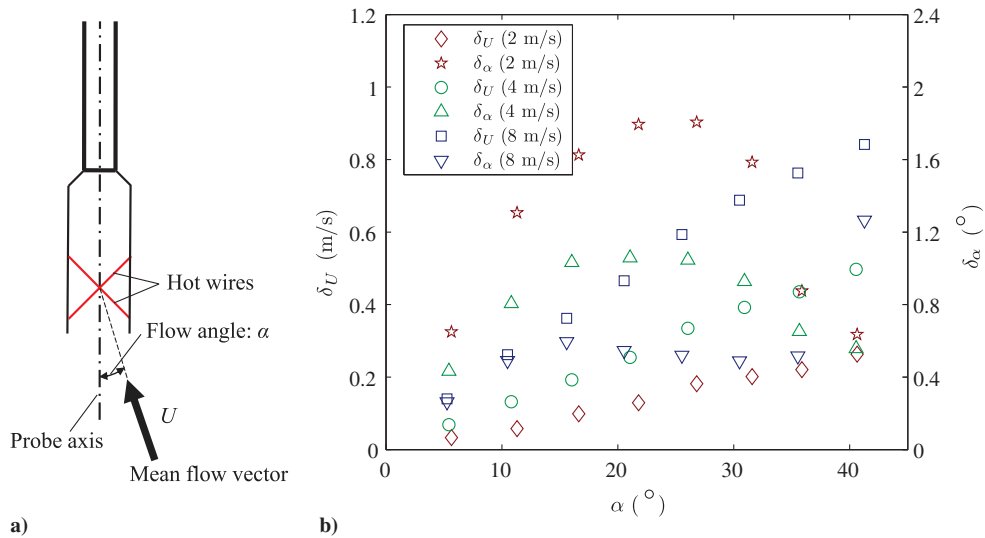


Fig. 4 a) A close-up schematic and b) errors of velocity measurement for the x-shaped hot-wire probe.

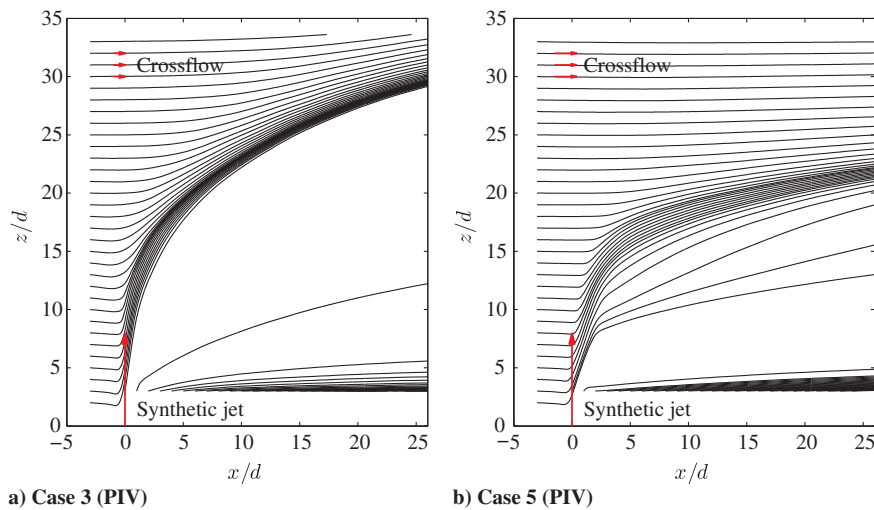


Fig. 5 The streamline plots for a) case 3: $w_j = 15.3$ m/s, $u_\infty = 2$ m/s, and b) case 5: $w_j = 16.7$ m/s, $u_\infty = 4$ m/s. w_{j2} estimated from Eq. (14) is used here as the effective jet velocity.

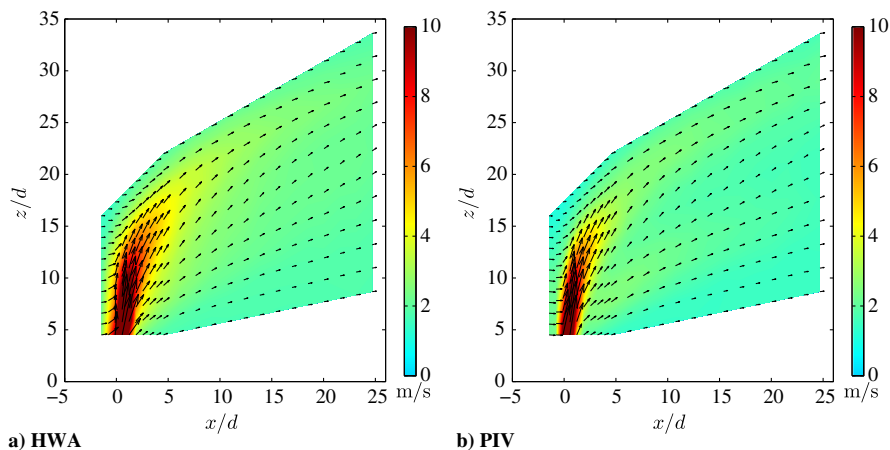


Fig. 6 Comparison of velocity vectors and magnitude contour between HWA and PIV measurements for case 3: $w_j = 15.3$ m/s, $u_\infty = 2$ m/s.

would begin its transition to turbulent flow and display self-similarity, the interaction between the jet and the crossflow starts to impact the entrainment of the jet so that the jet spreads and slightly bends toward the downstream direction. Nevertheless, the speed of the main jet flow is still significantly higher than its surrounding

crossflow, and so the dominant factor of the jet profile in this region is still the synthetic jet itself. The far field (III) is marked by the jet starting to bend significantly and the decay in speed of the main jet flow to a level that is comparable to the crossflow, so that the jet becomes merged within and dominated by the crossflow.

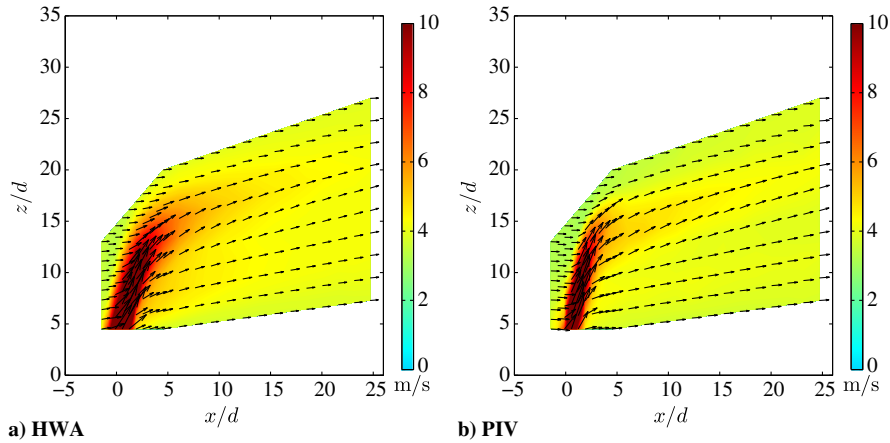


Fig. 7 Comparison of velocity vectors and magnitude contour between HWA and PIV measurements for case 5: $w_j = 16.7 \text{ m/s}$, $u_\infty = 4 \text{ m/s}$.

B. Jet Centerline Trajectory

The properties associated with the jet centerline, such as location and velocities, are the main focus of this study. The centerline here refers to the curve corresponding to the local maximum speed inside the main jet region. To accurately identify the centerline location with the experimentally obtained flow field, a contour-line-searching algorithm is used based on the velocity-magnitude contours, as illustrated in Fig. 8. Here, we first note that the PIV contour captures a secondary jet stream that does not appear in the HWA contour. Although more details are not presented here, we note that this

secondary jet stream is created by the trailing vortices, which are formed after the pinch-off [11] of the leading vortex rings. Again, this different flow feature likely reflects a finer spatial resolution of the PIV measurement and the spatial-averaging effect of the HWA measurement. The resultant centerline points are qualitatively divided into two groups, the near-field and the far-field, based on identifying the transitional region where the jet trajectory shows a notably different bending trend. The same can be done for the other cases and the results are compared in Fig. 9. A good agreement between the HWA and PIV results can be confirmed for all cases.

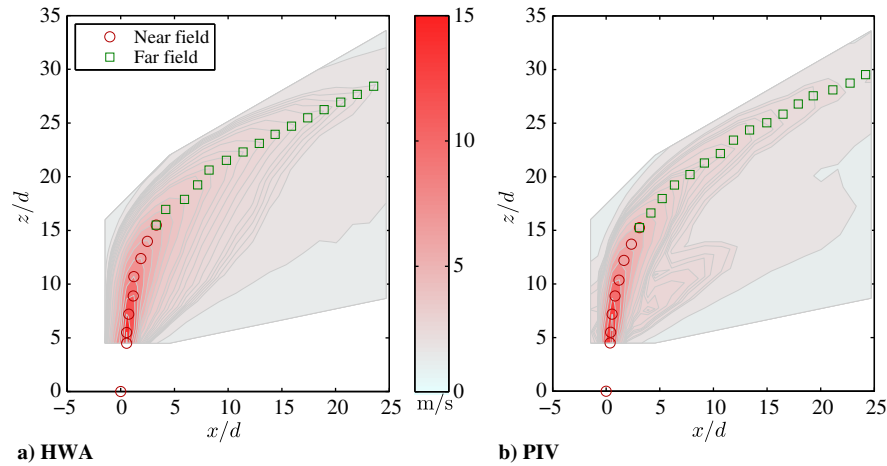


Fig. 8 Velocity-magnitude contours and calculated centerline points obtained from a) HWA and b) PIV measurements, respectively, for case 3.

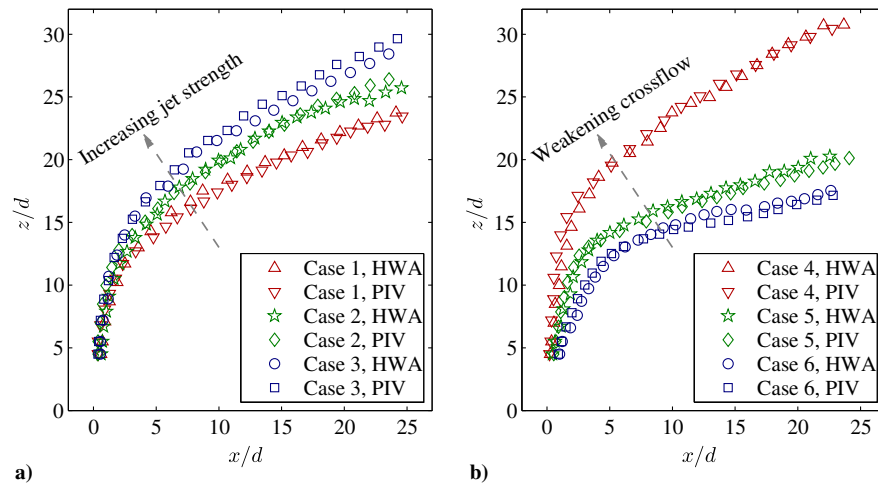


Fig. 9 The centerline points calculated from HWA and PIV data for a) cases 1–3 and b) cases 4–6.

Furthermore, we can conclude from Figs. 9a and 9b that both increasing jet strength and weakening crossflow will decrease the bending angle of the trajectory and increase the depth the jet flow penetrates into the crossflow.

IV. Theoretical Modeling

As both continuous jets and synthetic jets are self-similar in the far field, Krishnan and Mohseni [19] were able to model a round synthetic jet in a quiescent environment using the Schlichting jet solution [64,65], a model that was originally developed for a continuous jet. Following the same idea, this study seeks to extend the modeling approach of a transverse continuous jet to a transverse synthetic jet. This is achieved by adopting Hasselbrink and Mungal's model [59], which gives the similarity solutions of a transverse continuous jet by applying conservation equations to a control volume containing the mainstream of the jet in crossflow. By further defining an effective synthetic jet velocity in a momentum conservation sense, we obtain the similarity relations about the centerline trajectory and velocity for a transverse synthetic jet.

A. Scaling Laws for a Transverse Synthetic Jet

Figure 10 shows a schematic of the control volume including the transverse synthetic jet. Here, the objective is the jet centerline trajectory, which is defined to be the streamline corresponding to the local maximum speed inside the jet. Only the x -component velocity u and the z -component velocity w are considered because the centerline trajectory is a 2D property in the x - z plane. We define the position of the centerline to be $P(x_c, z_c)$, and the distance from origin to P along the centerline to be s .

To simplify the problem, the effect of the boundary layer is not considered and the crossflow velocity u_∞ is assumed to have a uniform profile, at least in the near field (II) and far field (III). In practice, this model requires the boundary layer to be contained inside the synthetic jet region (I). This is why the experiment is designed to have a thin laminar boundary layer as characterized in Fig. 3. Moreover, the span of the jet is assumed to be confined to a characteristic area A_s , such that $u \rightarrow u_\infty$ and $w \rightarrow 0$ outside the area A_s . This also means that A_s is the corresponding cross-sectional area that is perpendicular to the centerline of the jet. Here, we further assume that the total pressure integral of the background flow applied to this control volume is zero. Therefore, the conservation of the mass flux \dot{m} , z -momentum flux \dot{M}_z , and x -momentum deficit $\Delta\dot{M}_x$ through the cross section at a given distance s from the jet orifice can be expressed as

$$\dot{m}(s) := \int_{A_s} \rho \sqrt{(u^2 + w^2)} dA_s = \dot{m}_j + \dot{m}_\infty \quad (1)$$

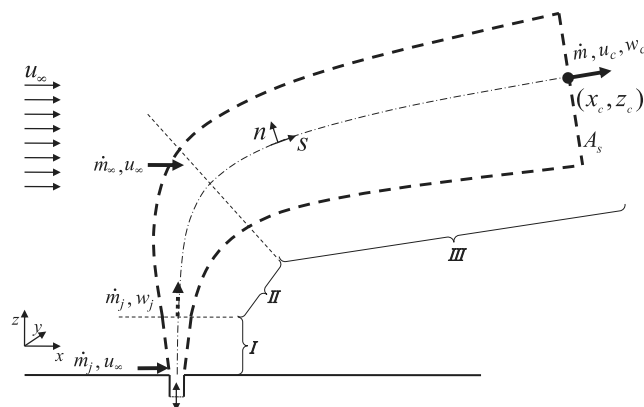


Fig. 10 Flow schematic and control volume for a transverse synthetic jet.

$$\dot{M}_z(s) := \int_{A_s} \rho w \sqrt{(u^2 + w^2)} dA_s = \dot{m}_j w_j \quad (2)$$

$$\Delta\dot{M}_x(s) := \int_{A_s} \rho (u_\infty - u) \sqrt{(u^2 + w^2)} dA_s = \dot{m}_j u_\infty \quad (3)$$

\dot{m}_∞ is the total mass flux of the ambient fluid entrained by the jet. w_j and \dot{m}_j are the effective jet velocity and effective jet mass flux, respectively, that are evaluated at the beginning of the near field (II) based on momentum conservation of the jet flow. Note here that the right-hand side of Eq. (3) is based on the jet mass flux \dot{m}_j entering the near field with $u = 0$.

The momentum balance equations imply that there are two invariants that characterize this jet flow: $\dot{M}_z = \dot{m}_j w_j$ and $\Delta\dot{M}_x = \dot{m}_j u_\infty$. It is, therefore, possible to perform similarity analysis based on one of the invariants. It should be pointed out that, unlike the transverse continuous jets where \dot{m}_j comes from an external flow source [59], \dot{m}_j of transverse synthetic jets is extracted from the crossflow. It is clearly seen from the momentum balance equations that the actuator is actually absorbing the x momentum of $\dot{m}_j u_\infty$ from the crossflow and converting that to z momentum of $\dot{m}_j w_j$ to generate the jet flow.

To extend the similarity analysis from continuous jets to synthetic jets in crossflow, we assume that the velocity ratio of jet to crossflow is large enough so that the jet reaches its self-similar region at the near field (II) of a transverse synthetic jet. Therefore, this means that self-similar jet regions exist in the near and far field for transverse synthetic jets with large velocity ratio. Next, dimensional analysis similar to Hasselbrink and Mungal [59] can be performed. This gives the scaling laws for the centerline trajectory as

$$\text{Near field: } \frac{z_c}{rd} = A_n \left(\frac{x_c}{rd} \right)^{1/2} \quad (4)$$

$$\text{Far field: } \frac{z_c}{rd} = A_f \left(\frac{x_c}{rd} \right)^{1/3} \quad (5)$$

where the subscript c denotes the properties associated with the jet centerline. Here, r is the jet-to-freestream velocity ratio, also known as the blowing ratio [48], which is defined as

$$r = \frac{w_j}{u_\infty} \quad (6)$$

Again, w_j is the effective synthetic jet velocity in a mean sense. The scaling relations for w and u of the centerline can be derived in the near field as

$$\frac{w_j}{w_c} = B_n \frac{z_c}{d} \quad (7)$$

$$\frac{u_\infty}{u_\infty - u_c} = C_n \frac{z_c}{d} \quad (8)$$

For the jet centerline in the far field, the scaling relations for w and u can be expressed as

$$\frac{w_j}{w_c} = B_f r \left(\frac{x_c}{rd} \right)^{2/3} \quad (9)$$

$$\frac{u_\infty}{u_\infty - u_c} = C_f r \left(\frac{x_c}{rd} \right)^{2/3} \quad (10)$$

The constants of proportionality A_n , A_f , B_n , and B_f are calculated from the experimental data as explained in the following sections. A_n and A_f quantify the amount of bending of the trajectory of a

Table 2 Effective jet velocities and velocity ratios for all cases

Case	w_{j1} , m/s	w_{j2} , m/s	r_1	r_2
1	14.0	11.3	7.0	5.6
2	18.6	13.0	9.3	6.5
3	24.7	15.3	12.3	7.7
4	29.9	16.7	14.9	8.3
5	29.9	16.7	7.5	4.2
6	29.9	16.7	5.0	2.8

r_1 and r_2 are estimated with w_j from Eqs. (11) and (14), respectively.

transverse synthetic jet in the near and far field, respectively. Larger values of the coefficients essentially correspond to less bending. B_n and B_f quantify the decay of the z -component velocity, where a larger value of the coefficient indicates a stronger decay behavior. It has been found that, for a continuous jet with large velocity ratio, $A_n, A_f, B_n,$ and B_f are constants (around 2.5, 1.6, 0.16, and 0.94, respectively) [59]. This suggests the existence of a common set of scaling laws for continuous jets. In this study, a main objective is to extend this unified model to synthetic jets and find the coefficients corresponding to the scaling laws.

Before we proceed, it is important to note that the scaling laws associated with the trajectory and the velocity w_c [Eqs. (4), (5), (7), and (9)] are obtained with the assumption of invariant \dot{M}_z , whereas the scaling laws associated with u_c [Eqs. (8) and (10)] are derived based on invariance of $\Delta\dot{M}_x$. Therefore, the validity of these two sets of scaling laws depends on the invariance of \dot{M}_z and $\Delta\dot{M}_x$, respectively. For the former, the following section will propose an effective jet velocity that conserves \dot{M}_z by nature. For the latter, its validity will be discussed in Sec. V.C.

B. Effective Jet Velocity and Velocity Ratio

The previous section adopts the scaling laws for a transverse continuous jet and applies a similar approach to the case of a synthetic jet. Essentially, this model is based upon the assumption that a constant momentum flux \dot{M}_z in the z direction is being added to the near field (II) of the transverse synthetic jet. As a result, an effective jet velocity, w_j , can be defined so that $\dot{M}_z = \dot{m}_j w_j$. However, contrary to the assumption, the momentum flux generated by a synthetic jet actuator is pulsed in nature. To account for the difference, a momentum-addition approach is incorporated into the model for synthetic jets.

Because the z -momentum flux is assumed to be conserved in the near and far field of a transverse jet, the averaged momentum flux at the jet exit should equal \dot{M}_z during an entire actuation period. Based on this model and a slug assumption that assumes the fluid to be ejected with a “top-hat” velocity profile at a constant rate during each

stroke, Krishnan and Mohseni [19] estimated the effective jet velocity at the jet exit of a synthetic jet to be

$$w_{j1} = \sqrt{2}fL \tag{11}$$

Based on this effective jet velocity, the jet-to-freestream velocity ratio r_1 is calculated using Eq. (6) and listed in Table 2.

Recently, Xia and Mohseni [16] demonstrated that, in the absence of crossflow, the far-field momentum flux of a round synthetic jet is always smaller than the prediction from the slug model. They further pointed out that the deceleration effect during the suction phase is one reason for the mismatch. The other is associated with the pinch-off process [11,12,66,67] that results in the generation of trailing vortical structures containing a much smaller momentum flux per unit circulation, in comparison with that of the leading vortex rings. They further showed that the primary contribution to the far-field momentum flux is the impulse carried by the fully-developed vortex ring formed during each stroke. Moreover, Jabbar and Zhong [43] also showed that the penetration and the core flow of a transverse synthetic jet are determined by the trajectory of the vortex rings. It can be implied from their study that the main-stream trajectory of a transverse synthetic jet is primarily attributable to the propagation of the leading vortex rings, whereas the trailing vortical structures move along trajectories away from the jet centerline, as shown in Fig. 1. From this notion, the initial momentum flux of the transverse synthetic jet may be calculated with the impulse of the vortex rings. Based on this model [16], \dot{M}_z in Eq. (2) could be calculated from

$$\dot{M}_z = \frac{\rho\pi^3}{32} f^2 d^2 L^2 \alpha_0^2 C \tag{12}$$

where $\alpha_0 = 1.2$ and C is the fraction of the total circulation in the vortex ring. C can be roughly estimated by

$$C = \begin{cases} 1 & \text{if } L/d < L^*/d \\ (L^*/d)/(L/d) & \text{if } L/d > L^*/d \end{cases} \tag{13}$$

where L^* is the characteristic stroke length associated with the jet formation number [11,12,16] for synthetic jets. Subsequently, the effective jet velocity w_j can be obtained by

$$w_{j2} = \frac{\sqrt{2C}}{4} \pi \alpha_0 f L \tag{14}$$

Thus, a novel jet-to-freestream velocity ratio, r_2 , is estimated with w_j from Eq. (14) and listed in Table 2. We now evaluate the performance of Eqs. (11) and (14) by comparing the predicted jet effective velocities with experimental data of the jet centerline velocities, as shown in Fig. 11. We can generally observe that the

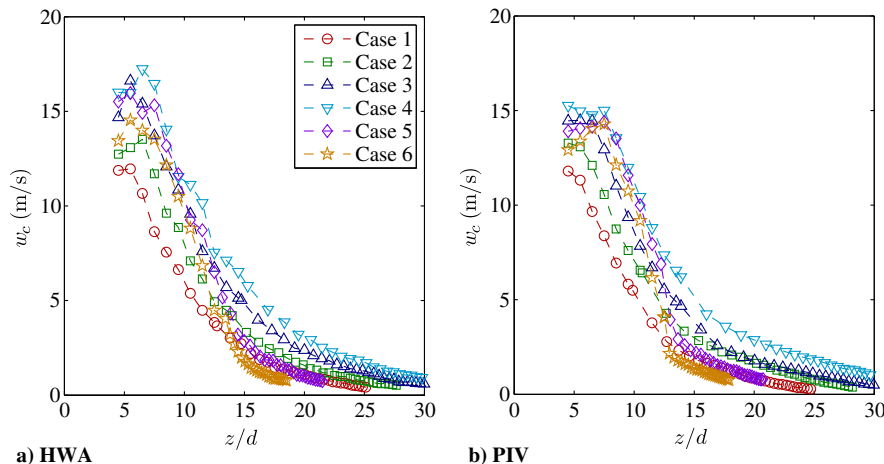


Fig. 11 Variation of time-averaged z -component velocity along the centerline for different transverse synthetic jets, obtained from a) HWA and b) PIV measurements.

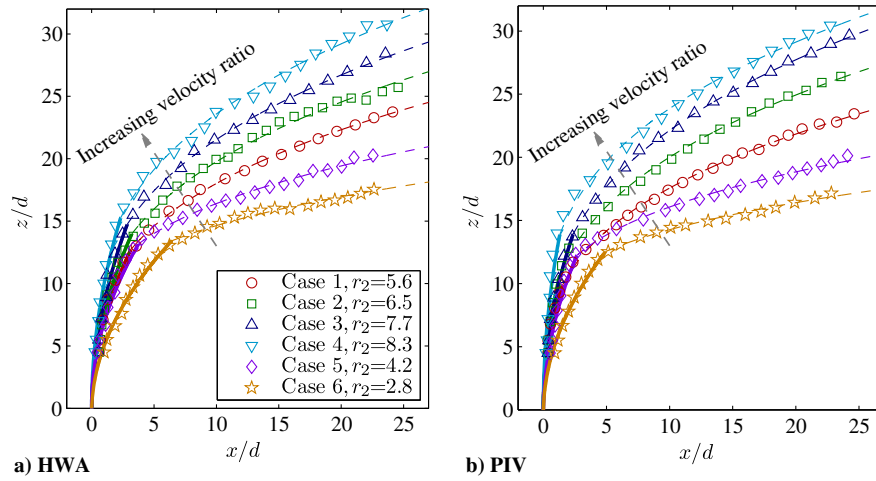


Fig. 12 The centerline trajectories (solid line and dashed line represent the near field and far field, respectively) obtained by fitting Eqs. (4) and (5) to the calculated centerline points in Fig. 9.

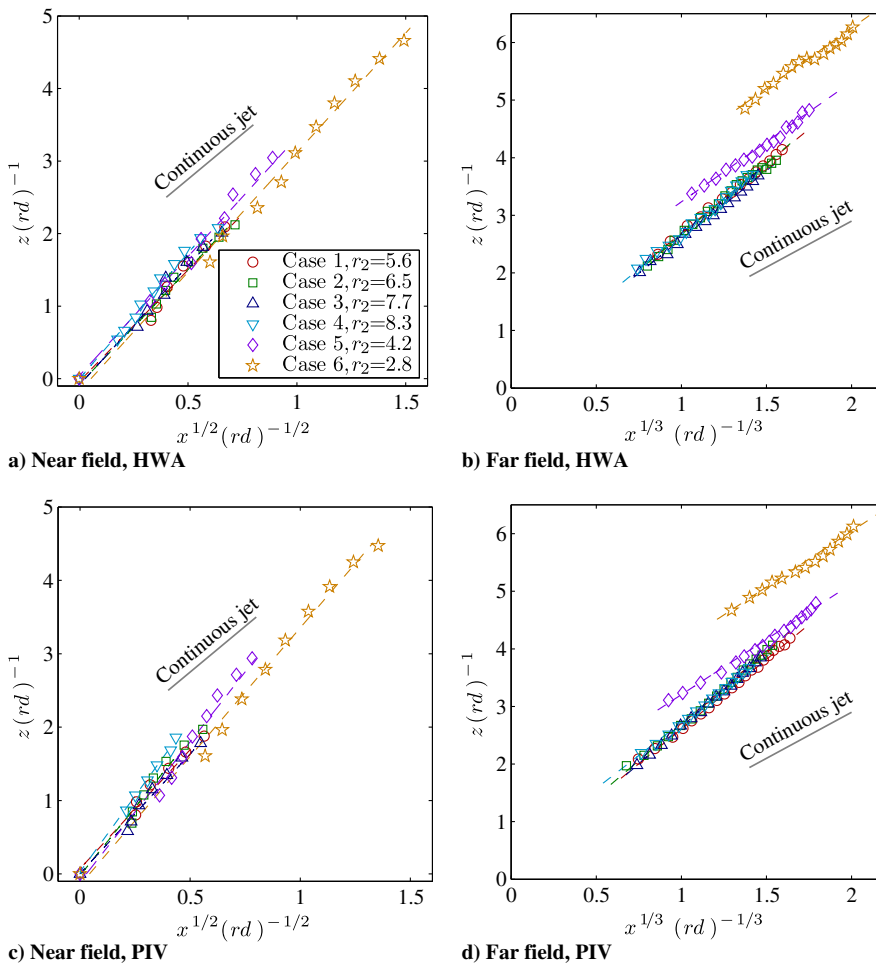


Fig. 13 Validation of the scaling relations [Eqs. (4) and (5) represented by the dashed lines] for the trajectory of transverse synthetic jets.

peak centerline velocities obtained from both HWA and PIV measurements are better predicted by w_{j2} . Therefore, the following analysis will be based on the effective jet velocity w_{j2} and the velocity ratio r_2 . It should be noted that although the overall agreement between the two measurements is good in the far field, the HWA data for some cases seem to measure slightly higher peak velocities in the near field compared with the PIV data. A similar observation has also been reported by Yehoshua and Seifert [44], who attributed the

different mean velocities to the differences in spatial and temporal resolutions between HWA and PIV measurements.

V. Model Validation

This section will provide validation of the scaling laws obtained in Sec. IV for the centerline trajectory and velocities of transverse synthetic jets, based on both HWA and PIV velocity field data. The

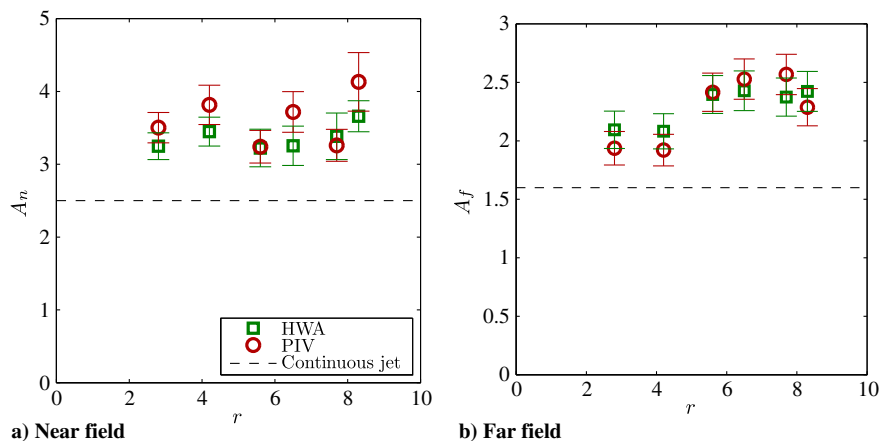


Fig. 14 The trajectory coefficient A_n and A_f and their error bars for the near field and far field, respectively.

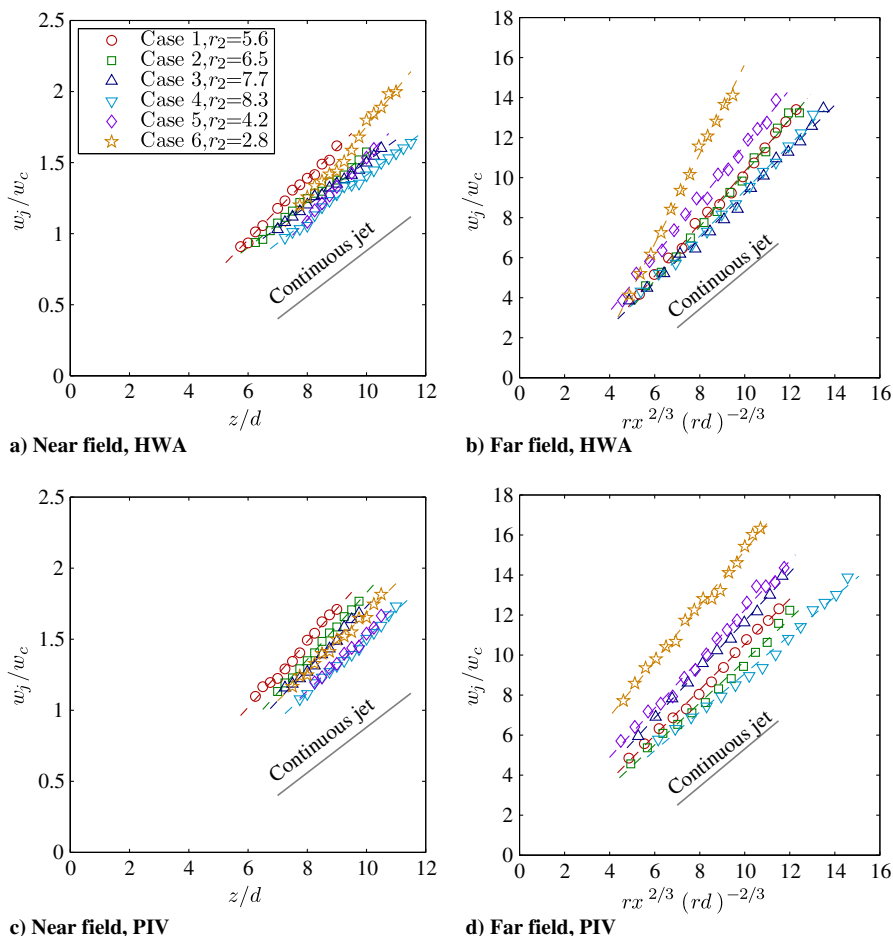


Fig. 15 Validation of the scaling relations [Eqs. (7) and (9) represented by the dashed lines] between the w velocity and the scaled location for the jet centerline.

objective here is to quantify the coefficients corresponding to the scaling laws and then verify the universality of the coefficients for transverse synthetic jets with different velocity ratios.

A. Trajectory Relations

The centerline trajectories have been obtained from flow field data in Sec. III.B. We now move on to verify the model proposed in Sec. IV by fitting Eqs. (4) and (5) to the centerline points in the near and far field, respectively. The results are shown in Fig. 12 and corresponds to the data presented in Fig. 9. It can be observed that the scaling laws presented in Eqs. (4) and (5) accurately capture the

centerline trajectories of different transverse synthetic jets. Furthermore, with the velocity ratio r_2 modeled in Sec. IV.B, we can confirm that the bending angle of the trajectory and the penetration depth are directly controlled by the jet-to-freestream velocity ratio as shown in Fig. 9.

Next, a direct comparison between the scaling laws [Eqs. (4) and (5)] and the trajectory data are provided in Fig. 13. Note that the slope of the lines in Fig. 13 corresponds to the fitting coefficients A_n and A_f for the near-field and far-field trajectories, respectively. Thus, we can evaluate the performance of the scaling laws by comparing the value of the fitting coefficients in Fig. 14. Again, A_n and A_f physically characterize the bending of a transverse synthetic jet, with a larger

value indicating less bending. The values of A_n and A_f for a continuous jet are about 2.5 and 1.6 [58,59], respectively. From Fig. 14, it can be observed that the A_n and A_f values are notably larger than the case of a continuous jet. This suggests that a synthetic jet is less apt to bend and penetrates further into the crossflow compared with an equivalent continuous jet that has the same velocity ratio. Lastly, because this model assumes large velocity ratio ($r \gg 1$) as a prerequisite for the dimensional analysis [59], it is expected that the model is better suited for large-velocity-ratio cases. This explains why cases 5 and 6 (with relatively small velocity ratio) in Figs. 13b and 13d do not collapse with the other cases in the far field. For this reason, A_n and A_f for transverse synthetic jets are determined to be 3.5 ± 0.4 and 2.4 ± 0.1 , respectively, based on the averaged values of cases 1–4.

B. z -Component Velocity Relations

The previous subsection has verified the scaling laws of Eqs. (4) and (5) that are associated with the centerline trajectory of a transverse synthetic jet. In this part, the focus is to study the variation of the z -component velocity along the centerline, and the scaling laws are proposed to be governed by Eqs. (7) and (9). The z component of the centerline velocity is required for these scaling laws, and it is calculated here by interpolating the w velocity field data.

We start with the z -component velocity, which is the velocity component perpendicular to the direction of the crossflow. For this velocity component, Fig. 15 shows the fitted linear relations of

Eqs. (7) and (9) for the near and far field. It can be observed from Fig. 15 that different lines collapse to a single slope. This observation can be further verified in Fig. 16, in which B_n and B_f show a good uniformity. It should be noted that cases with small r deviate from the converged values, that is, cases 5 and 6, in which the larger values of B_n and B_f indicate a faster decay rate of the w velocity. This, again, is consistent with the large-velocity-ratio assumption that affects the accuracy of the scaling laws when the velocity ratio is not high enough. Furthermore, Figs. 15 and 16 also show that B_n and B_f for transverse synthetic jets are comparable to those for a transverse continuous jet, for which $B_n \approx 0.16$ and $B_f \approx 0.94$ [59]. Therefore, based on the average of cases 1–4, B_n and B_f are estimated to be 0.19 ± 0.03 and 1.13 ± 0.06 , respectively, for transverse synthetic jets.

C. Synthetic-Jet Effect on the x -Component Velocity

The x -component velocity u is in the same direction as the crossflow. The scaling laws for u are given by Eqs. (8) and (10). Before proceeding to the validation, we first recall from Sec. IV.A that Eqs. (8) and (10) were derived based on assuming the x -momentum deficit ΔM_x being a constant. This is true for a continuous jet because the initial jet has only z -component velocity before entering the near field, and u would gradually increase to approach the crossflow velocity in the far field as the jet entrains ambient fluid moving at the speed of u_∞ . During this process, the x -momentum deficit associated with the initial jet persists throughout the entire transverse jet region. However, the

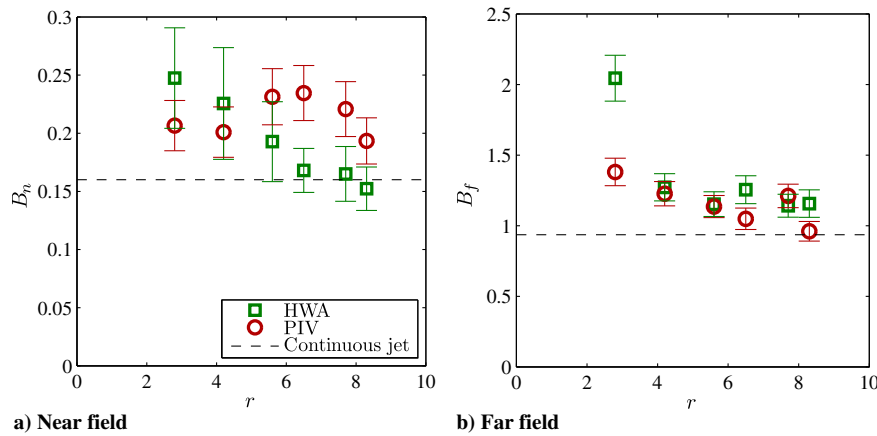


Fig. 16 The w -velocity coefficient B_n and B_f and their error bars for the centerline of the near field and far field, respectively.

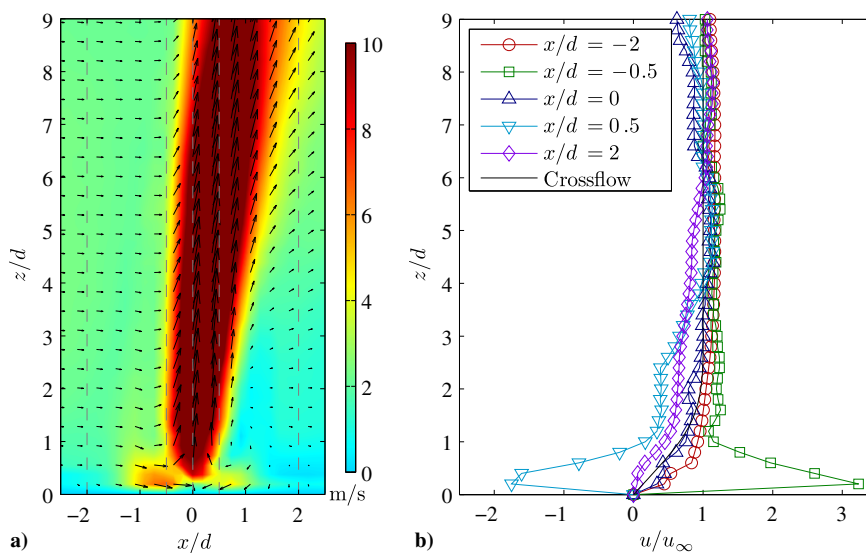


Fig. 17 a) Velocity magnitude contour and vector field of the mean flow (PIV) for case 3. b) Mean u -velocity profiles corresponding to the dashed lines in (a).

scenario is completely different for a synthetic jet in crossflow because of the induced effect of the formed vortical structures. To demonstrate how this affects the u velocity of a transverse synthetic jet, we first present the mean flow of the synthetic-jet formation region (I) and near field (II) for two sample cases (case 3: $r_2 = 7.7$, $u_\infty = 2$ m/s; case 5: $r_2 = 4.2$, $u_\infty = 4$ m/s) in Figs. 17 and 18, respectively. For clarity, the vector field of Figs. 17a and 18a are plotted on double-spaced grid compared to the original data.

We can observe from Figs. 17a and 18a that the mean velocity vectors of the main jet have a notable x component, which exists even at the root of the jet. This seems to indicate that the initial synthetic jet enters the near field with a nonzero u velocity, which differs from a continuous jet. This observation can be further justified in Figs. 17b and 18b, which show that the u velocity for a transverse synthetic jet quickly reaches or even exceeds u_∞ at a distance only $2d \sim 3d$ away from the jet exit. As a result, the constant x -momentum deficit between the jet and the crossflow does not hold for a transverse synthetic jet, which means that the scaling laws of Eqs. (8) and (10) are not suitable here. Before we move on to explain the mechanism causing the nonzero u velocity in the near field of a transverse

synthetic jet, we emphasize that the validity of the x -momentum deficit assumption does not affect the trajectory and the w scaling laws. This is because these two relations were derived based on the assumption of invariant z momentum only, as discussed in Sec. IV.A.

To further understand the different behaviors of the u velocity for a transverse synthetic jet, we present the instantaneous vorticity and vector fields for case 3 and case 5 in Figs. 19 and 20, respectively. Again, we emphasize that u for a transverse continuous jet is approximately zero near the jet exit as the crossflow is intersected by the continuous jetting flow in the perpendicular direction; however, this is not the case for a synthetic jet because the crossflow near the jet exit can be recovered during the suction period, as can be observed from Figs. 19a and 20a. This partly explains the positive u value of the mean flow in Figs. 17 and 18. Still, this recovery mechanism does not fully justify the observation of Figs. 17b and 18b, in which the mean u velocity in the jet region can be significantly larger than u_∞ .

At this point, it is natural to connect the enhanced u velocity to the vortex rings of the synthetic jet. As can be observed in Figs. 19 and 20, the downstream part (right) of the vortex ring has a negative net vorticity, and induces a positive u velocity in the neighborhood above

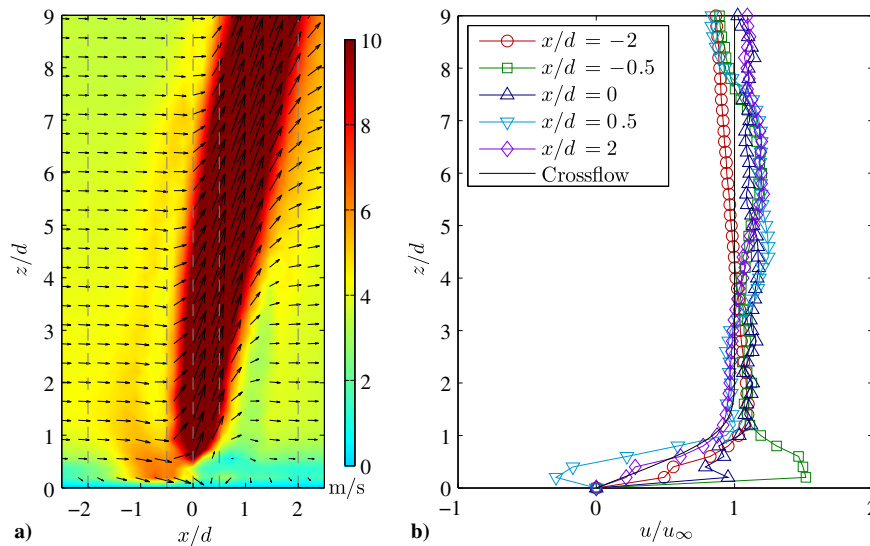


Fig. 18 a) Velocity magnitude contour and vector field of the mean flow (PIV) for case 5. b) Mean u -velocity profiles corresponding to the dashed lines in (a).

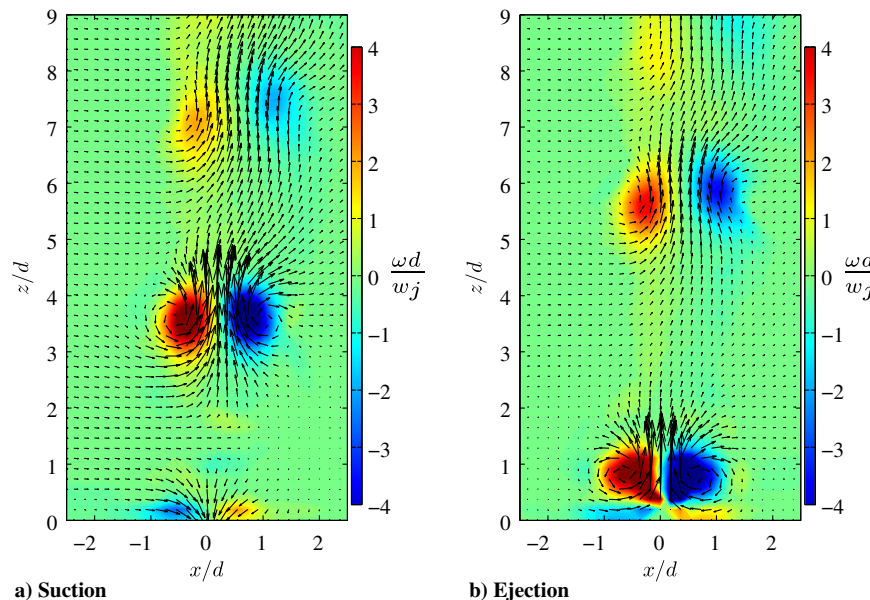


Fig. 19 The vorticity contour and vector field of the instantaneous jet flow for a) suction and b) ejection phases of case 3 shown in Fig. 17. Here, the vorticity is scaled by w_j/d .

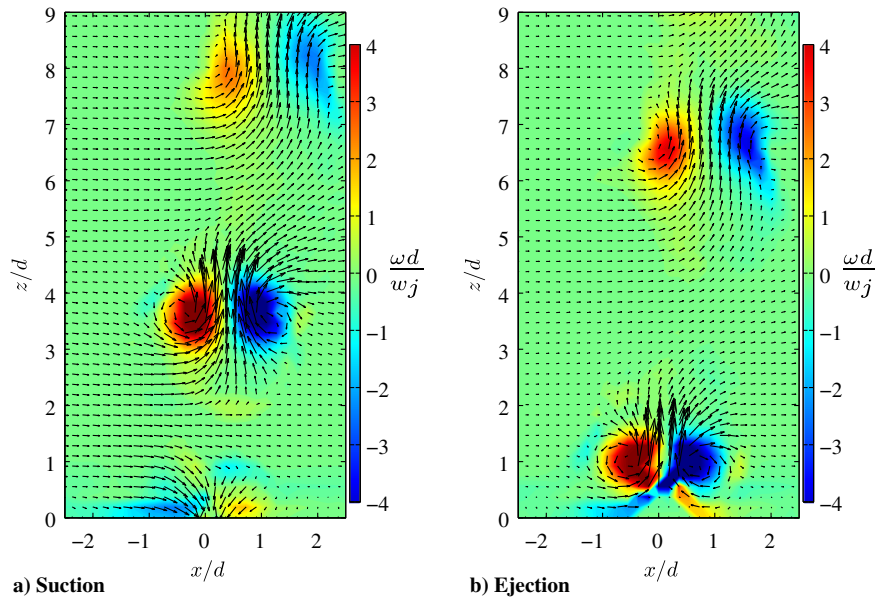


Fig. 20 The vorticity contour and vector field of the instantaneous jet flow for a) suction and b) ejection phases of case 5 shown in Fig. 18.

and a negative u velocity in the neighborhood below. On the contrary, the upstream part of the vortex ring induces a positive u velocity below it and a negative u velocity above it. Thus, the total induced u velocity should be symmetric in the mean sense for a synthetic jet in a quiescent environment. However, for a synthetic jet in crossflow, these induced effects cause the crossflow to be enhanced in the regions below the upstream-part (left) vortex ring and above the downstream-part vortex ring, which is evident from the velocity vectors near the vortex rings (vortex pairs in the 2D plot) shown in Figs. 19 and 20. Based on this observation, we can conclude that the interactions between the crossflow and the vortex ring result in an asymmetrically induced effect of the vortex ring, which is eventually translated into an enhanced mean u velocity. Because of this asymmetrically enhanced flow in the vicinity of the vortex ring, the vortex ring axis also becomes tilted, as has been reported by Jabbal and Zhong [43]. The finding of the increased crossflow velocity in the near field indicates that the interaction between the synthetic jet and the crossflow also enhances the flow momentum outside the boundary layer. This could be an auxiliary contribution to the momentum mixing mechanism that has been proposed to cause delay of flow separation [36–39].

Lastly, we note that the effect of the crossflow boundary layer on the formation and evolution of the vortex ring is marginal in this study. According to Yehoshua and Seifert [44] and Jabbal and Zhong [43], the established vorticity field associated with the boundary layer would cancel out the vorticity of the upstream part of the vortex ring and adds to the vorticity of the downstream part, which might create further asymmetric enhancement of the u velocity. However, in the current study of strong synthetic jet versus weak crossflow, the average nondimensional vorticity, $\bar{\omega}d/w_j$, for the boundary layer is around 0.1 and the thickness is less than $3d$. In this case, the vorticity distribution of the vortex ring is hardly affected by the weak and thin boundary layer. Quantitatively, for the fully generated vortex ring located at the center of Fig. 19a, the nondimensional circulation, $\Gamma/(w_jd)$, corresponding to the upstream part and the downstream part are calculated to be 2.68 and -2.60 , respectively, using the Q -criterion [68]. Similarly, the two circulations for the fully developed vortex ring in Fig. 20a are estimated to be 2.90 and -2.99 , respectively. Therefore, the small difference between the circulations of the upstream-part and downstream-part vortex ring demonstrates a small influence of the crossflow boundary layer.

VI. Conclusions

The flow field of strong synthetic jets in crossflow is investigated using HWA and PIV. An automated rotary stage together with an

iterative angle-finding algorithm is adopted to improve the accuracy of the HWA. Similarity analysis is successfully extended from continuous jets to model the centerline trajectory and velocity of synthetic jets in crossflow, based on the two invariants of the flow, the z -direction momentum and x -direction momentum deficit. Experimental data are used to validate the scaling laws for the centerline velocity and trajectory of the jet, with different jet-to-freestream velocity ratios being tested. The HWA and PIV measurements generally have a good matching with each other for the tested mean velocity field of transverse jet. However, because of the spatial averaging effect, the HWA anemometry tends to measure a larger jet region. It is found that the effective jet velocity is better predicted in a momentum conservation sense, based on the momentum flux of the leading vortex rings instead of the momentum flux of the ejected slug at the jet exit.

The scaling laws for the trajectory and the z -component velocity of a transverse synthetic jet are given by Eqs. (4), (5), (7), and (9), whereas the corresponding coefficients, A_n , A_f , B_n , and B_f , are determined to be 3.5, 2.4, 0.19, and 1.13, respectively. These scaling coefficients show good consistency for different synthetic jets with large velocity ratios, whereas significant variation of the coefficients can be observed for the small-velocity-ratio cases. This observation is consistent with the basic assumption of the scaling laws that the jet-to-velocity ratio should be significantly larger than unity. By comparing the scaling coefficients for the centerline trajectory between synthetic jets and continuous jets, it is concluded that a synthetic jet is less likely to deflect and penetrates further than a continuous jet.

Another finding of this study is that the u velocity of a transverse synthetic jet displays a dramatic difference from that of a continuous jet. Specifically, u is observed to be notably increased in the near field of a transverse synthetic jet, whereas u for a continuous jet is approximately zero in the same region. Thus, the scaling laws for the u velocity are not applicable for the case of a transverse synthetic jet. This increased u velocity can be attributed to an asymmetric induced effect by the vortex rings, and it indicates an enhanced momentum of the crossflow outside the boundary layer. Therefore, the enhanced crossflow could provide additional contribution to enhancing momentum inside the boundary layer and delaying flow separation, by means of momentum mixing across the boundary layer.

Acknowledgments

This work is supported by a grant from the Office of Naval Research. We are grateful to the referees for their valuable comments that lead to great improvements of this paper. We would like to

appreciate Adam DeVoria and Thomas Linehan for their assistance in setting up the particle image velocimetry experiment. We would like to thank Michael Kreig, Yiming Xu, and Peter Zhang for their helpful comments.

References

- [1] Smith, B. L., and Glezer, A., "The Formation and Evolution of Synthetic Jets," *Physics of Fluids*, Vol. 10, No. 9, 1998, pp. 2281–2297. doi:10.1063/1.869828
- [2] Glezer, A., and Amitay, M., "Synthetic Jets," *Annual Review of Fluid Mechanics*, Vol. 34, No. 1, 2002, pp. 503–529. doi:10.1146/annurev.fluid.34.090501.094913
- [3] Cattafesta, L. N., and Sheplak, M., "Actuators for Active Flow Control," *Annual Review of Fluid Mechanics*, Vol. 43, No. 1, 2011, pp. 247–272. doi:10.1146/annurev-fluid-122109-160634
- [4] Mohseni, K., and Mittal, R., *Synthetic Jets: Fundamentals and Applications*, CRC Press, Boca Raton, FL, 2014, Chaps. 1, 6, 9, 10.
- [5] O'Dor, R. K., "The Forces Acting on Swimming Squid," *Journal of Experimental Biology*, Vol. 137, No. 1, 1988, pp. 421–442.
- [6] Krieg, M., and Mohseni, K., "Thrust Characterization of a Bioinspired Vortex Ring Thruster for Locomotion of Underwater Robots," *IEEE Journal of Oceanic Engineering*, Vol. 33, No. 2, 2008, pp. 123–132. doi:10.1109/JOE.2008.920171
- [7] Maxworthy, T., "Some Experimental Studies of Vortex Rings," *Journal of Fluid Mechanics*, Vol. 81, No. 3, 1977, pp. 465–495. doi:10.1017/S0022112077002171
- [8] Saffman, P. G., "The Number of Waves on Unstable Vortex Rings," *Journal of Fluid Mechanics*, Vol. 84, No. 4, 1978, pp. 625–639. doi:10.1017/S0022112078000385
- [9] Didden, N., "On the Formation of Vortex Rings: Rolling-Up and Production of Circulation," *Zeitschrift für Angewandte Mathematik und Physik*, Vol. 30, No. 1, 1979, pp. 101–116. doi:10.1007/BF01597484
- [10] Glezer, A., "The Formation of Vortex Rings," *Physics of Fluids*, Vol. 31, No. 12, 1988, pp. 3532–3542. doi:10.1063/1.866920
- [11] Gharib, M., Rambod, E., and Shariff, K., "A Universal Time Scale for Vortex Ring Formation," *Journal of Fluid Mechanics*, Vol. 360, 1998, pp. 121–140. doi:10.1017/S0022112097008410
- [12] Mohseni, K., and Gharib, M., "A Model for Universal Time Scale of Vortex Ring Formation," *Physics of Fluids*, Vol. 10, No. 10, 1998, pp. 2436–2438. doi:10.1063/1.869785
- [13] Rosenfeld, M., Rambod, E., and Gharib, M., "Circulation and Formation Number of Laminar Vortex Rings," *Journal of Fluid Mechanics*, Vol. 376, 1998, pp. 297–318. doi:10.1017/S0022112098003115
- [14] Smith, B. L., and Swift, G. W., "Synthetic Jets at Larger Reynolds Number and Comparison to Continuous Jets," AIAA Paper 2001-3030, June 2001.
- [15] Holman, R., Utturkar, Y., Mittal, R., Smith, B. L., and Cattafesta, L., "Formation Criterion for Synthetic Jets," *AIAA Journal*, Vol. 43, No. 10, 2005, pp. 2110–2116. doi:10.2514/1.12033
- [16] Xia, X., and Mohseni, K., "Far-Field Momentum Flux of High-Frequency Axisymmetric Synthetic Jets," *Physics of Fluids*, Vol. 27, No. 11, 2015, Paper 115101. doi:10.1063/1.4935011
- [17] Xia, X., and Mohseni, K., "Parameter Governing the Far-Field Features of Round Jets," *Physical Review Fluids*, Vol. 1, No. 6, 2016, Paper 062401.
- [18] Mallinson, S. G., Hong, G., and Reizes, J. A., "Some Characteristics of Synthetic Jets," AIAA Paper 1999-3651, 1999.
- [19] Krishnan, G., and Mohseni, K., "Axisymmetric Synthetic Jets: An Experimental and Theoretical Examination," *AIAA Journal*, Vol. 47, No. 10, 2009, pp. 2273–2283. doi:10.2514/1.42967
- [20] Krishnan, G., and Mohseni, K., "An Experimental and Analytical Investigation of Rectangular Synthetic Jets," *ASME Journal of Fluids Engineering*, Vol. 131, No. 12, 2009, Paper 121101. doi:10.1115/1.4000422
- [21] Cater, J. E., and Soria, J., "The Evolution of Round Zero-Net-Mass-Flux Jets," *Journal of Fluid Mechanics*, Vol. 472, 2002, pp. 167–200. doi:10.1017/S0022112002002264
- [22] Smith, B. L., and Swift, G. W., "A Comparison Between Synthetic Jets and Continuous Jets," *Experiments in Fluids*, Vol. 34, No. 4, 2003, pp. 467–472. doi:10.1007/s00348-002-0577-6
- [23] Mohseni, K., "Pulsatile Vortex Generators for Low-Speed Maneuvering of Small Underwater Vehicles," *Ocean Engineering*, Vol. 33, No. 16, 2006, pp. 2209–2223. doi:10.1016/j.oceaneng.2005.10.022
- [24] Seifert, A., Bachar, T., Koss, D., Shepshelovich, M., and Wygnanski, I., "Oscillatory Blowing: A Tool to Delay Boundary-Layer Separation," *AIAA Journal*, Vol. 31, No. 11, 1993, pp. 2052–2060. doi:10.2514/3.49121
- [25] Amitay, M., and Glezer, A., "Role of Actuation Frequency in Controlled Flow Reattachment over a Stalled Airfoil," *AIAA Journal*, Vol. 40, No. 2, 2002, pp. 209–216. doi:10.2514/2.1662
- [26] Amitay, M., and Glezer, A., "Controlled Transients of Flow Reattachment over Stalled Airfoils," *International Journal of Heat and Fluid Flow*, Vol. 23, No. 5, 2002, pp. 690–699. doi:10.1016/S0142-727X(02)00165-0
- [27] Yehoshua, T., and Seifert, A., "Active Boundary Layer Tripping Using Oscillatory Vorticity Generator," *Aerospace Science and Technology*, Vol. 10, No. 3, 2006, pp. 175–180. doi:10.1016/j.ast.2005.10.007
- [28] Zhang, S., and Zhong, S., "Experimental Investigation of Flow Separation Control Using an Array of Synthetic Jets," *AIAA Journal*, Vol. 48, No. 3, 2010, pp. 611–623. doi:10.2514/1.43673
- [29] Seifert, A., Eliahu, S., Greenblatt, D., and Wygnanski, I., "Use of Piezoelectric Actuators for Airfoil Separation Control," *AIAA Journal*, Vol. 36, No. 8, 1998, pp. 1535–1537. doi:10.2514/2.549
- [30] Amitay, M., Smith, D. R., Kibens, V., Parekh, D. E., and Glezer, A., "Aerodynamic Flow Control over an Unconventional Airfoil Using Synthetic Jet Actuators," *AIAA Journal*, Vol. 39, No. 3, 2001, pp. 361–370. doi:10.2514/2.1323
- [31] Mittal, R., and Rampunggoon, P., "On the Virtual Aeroshaping Effect of Synthetic Jets," *Physics of Fluids*, Vol. 14, No. 4, 2002, pp. 1533–1536. doi:10.1063/1.1453470
- [32] Gilarranz, J. L., Traub, L. W., and Rediniotis, O. K., "A New Class of Synthetic Jet Actuators—Part II: Application to Flow Separation Control," *ASME Journal of Fluids Engineering*, Vol. 127, No. 2, 2005, pp. 377–387. doi:10.1115/1.1882393
- [33] Raju, R., Mittal, R., and Cattafesta, L., "Dynamics of Airfoil Separation Control Using Zero-Net-Mass-Flux Forcing," *AIAA Journal*, Vol. 46, No. 12, 2008, pp. 3103–3115. doi:10.2514/1.37147
- [34] Williams, D., Kerstens, W., Pfeiffer, J., King, R., and Colonius, T., "Unsteady Lift Suppression with a Robust Closed Loop Controller," *Active Flow Control II*, edited by King, R., Springer, Berlin, 2010, pp. 19–30.
- [35] Zhang, Q., and Bodony, D. J., "Numerical Simulation of Two-Dimensional Acoustic Liners with High-Speed Grazing Flow," *AIAA Journal*, Vol. 49, No. 2, 2011, pp. 365–382. doi:10.2514/1.J050597
- [36] Smith, D. R., "Interaction of a Synthetic Jet with a Crossflow Boundary Layer," *AIAA Journal*, Vol. 40, No. 11, 2002, pp. 2277–2288. doi:10.2514/2.1564
- [37] Jabbal, M., and Zhong, S., "The Near Wall Effect of Synthetic Jets in a Boundary Layer," *International Journal of Heat and Fluid Flow*, Vol. 29, No. 1, 2008, pp. 119–130. doi:10.1016/j.ijheatfluidflow.2007.07.011
- [38] Zhong, S., and Zhang, S., "Further Examination of the Mechanism of Round Synthetic Jets in Delaying Turbulent Flow Separation," *Flow, Turbulence, and Combustion*, Vol. 91, No. 1, 2013, pp. 177–208. doi:10.1007/s10494-013-9469-5
- [39] Wen, X., and Tang, H., "On Hairpin Vortices Induced by Circular Synthetic Jets in Laminar and Turbulent Boundary Layers," *Computers and Fluids*, Vol. 95, 2014, pp. 1–18. doi:10.1016/j.compfluid.2014.02.002
- [40] Smith, D. R., Amitay, M., Kibens, V., Parekh, D., and Glezer, A., "Modification of Lifting Body Aerodynamics Using Synthetic Jet Actuators," *Proceedings of the AIAA Aerospace Sciences Meeting and Exhibit*, AIAA Paper 1998-0209, Jan. 1998.
- [41] Duvigneau, R., and Visonneau, M., "Simulation and Optimization of Stall Control for an Airfoil with a Synthetic Jet," *Aerospace Science and Technology*, Vol. 10, No. 4, 2006, pp. 279–287. doi:10.1016/j.ast.2006.01.002
- [42] Mittal, R., Rampunggoon, P., and Udaykumar, H. S., "Interaction of a Synthetic Jet with a Flat Plate Boundary Layer," *Proceedings of the AIAA Computational Fluid Dynamics Conference*, AIAA Paper 2001-2773, June 2001.

- [43] Jabbal, M., and Zhong, S., "Particle Image Velocimetry Measurements of the Interaction of Synthetic Jets with a Zero-Pressure Gradient Laminar Boundary Layer," *Physics of Fluids*, Vol. 22, No. 6, 2010, Paper 063603.
doi:10.1063/1.3432133
- [44] Yehoshua, T., and Seifert, A., "Boundary Condition Effects on Oscillatory Momentum Generators," *Proceedings of the 33rd AIAA Fluid Dynamics Conference and Exhibit*, AIAA Paper 2003-3710, June 2003.
- [45] Milanovic, I. M., and Zaman, K. B. M. Q., "Synthetic Jets in Crossflow," *AIAA Journal*, Vol. 43, No. 5, 2005, pp. 929–940.
doi:10.2514/1.4714
- [46] Schaeffler, N. W., and Jenkins, L. N., "Isolated Synthetic Jet in Crossflow: Experimental Protocols for a Validation Dataset," *AIAA Journal*, Vol. 44, No. 12, 2006, pp. 2846–2856.
doi:10.2514/1.13743
- [47] Ramasamy, M., Wilson, J. S., and Martin, P. B., "Interaction of Synthetic Jet with Boundary Layer Using Microscopic Particle Image Velocimetry," *Journal of Aircraft*, Vol. 47, No. 2, 2010, pp. 404–422.
doi:10.2514/1.45794
- [48] Sahni, O., Wood, J., Jansen, K. E., and Amitay, M., "Three-Dimensional Interactions Between a Finite-Span Synthetic Jet and a Crossflow," *Journal of Fluid Mechanics*, Vol. 671, 2011, pp. 254–287.
doi:10.1017/S0022112010005604
- [49] Yehoshua, T., and Seifert, A., "Empirical Model for the Evolution of a Vortex-Pair Introduced into a Boundary Layer," *AerospaceLab*, No. 6, 2013, pp. 1–12.
- [50] Rumsey, C., Gatski, T., Sellers, W., Vatsa, V., and Viken, S., "Summary of the 2004 Computational Fluid Dynamics Validation Workshop on Synthetic Jets," *AIAA Journal*, Vol. 44, No. 2, 2006, pp. 194–207.
doi:10.2514/1.12957
- [51] Dandois, J., Garnier, E., and Sagaut, P., "Unsteady Simulation of a Synthetic Jet in a Crossflow," *AIAA Journal*, Vol. 44, No. 2, 2006, pp. 225–238.
doi:10.2514/1.13462
- [52] Rumsey, C. L., Schaeffler, N. W., Milanovic, I. M., and Zaman, K. B. M. Q., "Time-Accurate Computations of Isolated Circular Synthetic Jets in Crossflow," *Computers and Fluids*, Vol. 36, No. 6, 2007, pp. 1092–1105.
doi:10.1016/j.compfluid.2006.09.002
- [53] Zhou, J., and Zhong, S., "Numerical Simulation of the Interaction of a Circular Synthetic Jet with a Boundary Layer," *Computers and Fluids*, Vol. 38, No. 2, 2009, pp. 393–405.
doi:10.1016/j.compfluid.2008.04.012
- [54] Wu, D. K. L., and Leschziner, M. A., "Large-Eddy Simulations of Circular Synthetic Jets in Quiescent Surroundings and in Turbulent Cross-Flow," *International Journal of Heat and Fluid Flow*, Vol. 30, No. 3, 2009, pp. 421–434.
doi:10.1016/j.ijheatfluidflow.2009.01.007
- [55] Gordon, M., and Soria, J., "Scalar Mixing of Zero-Net-Mass-Flux Jets in Crossflow," *Proceedings of the 14th Australasian Fluid Mechanics Conference*, Australasian Fluid Mechanics Soc., Adelaide, SA, Dec. 2001, pp. 729–732.
- [56] Ugrina, S., "Experimental Analysis and Analytical Modeling of Synthetic Jet-Cross Flow Interactions," Ph.D. Thesis, Univ. of Maryland, College Park, MD, 2007.
- [57] Xia, X., and Mohseni, K., "Modeling and Experimental Investigation of Synthetic Jets in Cross-Flow," AIAA Paper 2010-0106, Jan. 2010.
- [58] Paul, C., "Mixing of Turbulent Advected Line Puffs," Ph.D. Thesis, Univ. of Hong Kong, Hong Kong, June 1996.
- [59] Hasselbrink, E. F., and Mungal, M. G., "Transverse Jets and Jet Flames. Part 1. Scaling Laws for Strong Transverse Jets," *Journal of Fluid Mechanics*, Vol. 443, 2001, pp. 1–25.
- [60] Xia, X., and Mohseni, K., "An Experimental and Modeling Investigation of Synthetic Jets in a Coflow Wake," *International Journal of Flow Control*, Vol. 3, No. 1, 2011, pp. 19–36.
doi:10.1260/1756-8250.3.1.19
- [61] Gordon, M., and Soria, J., "PIV Measurements of a Zero-Net-Mass-Flux-Jet in Cross Flow," *Experiments in Fluids*, Vol. 33, No. 6, 2002, pp. 863–872.
doi:10.1007/s00348-002-0518-4
- [62] Johnstone, A., Uddin, M., and Pollard, A., "Calibration of Hot-Wire Probes Using Non-Uniform Mean Velocity Profiles," *Experiments in Fluids*, Vol. 39, No. 3, 2005, pp. 527–534.
doi:10.1007/s00348-005-0972-x
- [63] Jorgensen, F. E., *How to Measure Turbulence with Hot-Wire Anemometers*, Dantec Dynamics, Denmark, 2005, Chap. 7.
- [64] Schlichting, H., "Laminare Strahlausbreitung," *Journal of Applied Mathematics and Mechanics*, Vol. 13, No. 4, 1933, pp. 260–263.
- [65] Schlichting, H., *Boundary Layer Theory*, 2nd ed., McGraw-Hill, New York, 1955, Chap. XXIII (23).
- [66] Shusser, M., and Gharib, M., "Energy and Velocity of a Forming Vortex Ring," *Physics of Fluids*, Vol. 12, No. 3, 2000, pp. 618–621.
doi:10.1063/1.870268
- [67] Mohseni, K., Ran, H., and Colonius, T., "Numerical Experiments on Vortex Ring Formation," *Journal of Fluid Mechanics*, Vol. 430, 2001, pp. 267–282.
doi:10.1017/S0022112000003025
- [68] Chakraborty, P., Balachandar, S., and Adrian, R. J., "On the Relationships Between Local Vortex Identification Schemes," *Journal of Fluid Mechanics*, Vol. 535, 2005, pp. 189–214.
doi:10.1017/S0022112005004726

I. Gursul
Associate Editor